Article

Seaweed-Derived Biochar for Effective Treatment of Dye-Contaminated Wastewater

Ana Paula Soares Dias [1,2,*], Francisco Ascenção Santos [3], Bruna Rijo [2], Dina Costa Simes [4], Leonel Pereira [5] and Manuel Francisco Costa Pereira [1]

1. CERENA, Center for Natural Resources and Environment, Instituto Superior Técnico, Universidade de Lisboa, Av. Rovisco Pais, 1, 1049-001 Lisbon, Portugal; mfcp@tecnico.ulisboa.pt
2. VALORIZA—Research Centre for Endogenous Resource Valorization, Polytechnic Institute of Portalegre, 7300-555 Portalegre, Portugal; bruna.rijo@ipportalegre.pt
3. Instituto Superior Técnico, Universidade de Lisboa, Av. Rovisco Pais, 1, 1049-001 Lisbon, Portugal; francisco.carreira.santos@tecnico.ulisboa.pt
4. CCMAR, Centre of Marine Sciences, Universidade do Algarve, Estr. da Penha, 8005-139 Faro, Portugal; dsimes@ualg.pt
5. Department of Life Sciences, University of Coimbra, Calçada Martim de Freitas, 3000-456 Coimbra, Portugal; leonel@bot.uc.pt
* Correspondence: apsoares@tecnico.ulisboa.pt; Tel.: +351-218417873

Abstract: Freshwater scarcity is a growing concern, exacerbated by industrial effluents containing dyes and other pollutants that endanger aquatic ecosystems. This study explores the potential of biochar sorbents, derived from renewable seaweed biomass, as a sustainable solution for water decontamination. Seaweed biomass (*sargaço*), collected from Portuguese seashores, was carbonized at 300 °C and 400 °C to produce biochar. Adsorption experiments with methylene blue (MB) revealed that carbonization at 400 °C, followed by ball milling, significantly enhanced adsorption performance. Langmuir isotherm analysis demonstrated a maximum adsorption capacity of 500 mg MB/g sorbent for the optimized biochar (400 °C, ball milled), with adsorption efficiency improving at elevated temperatures and pH levels up to 12. Infrared reflectance spectra of fresh and post-adsorption biochars confirmed the involvement of π–π interactions and hydrogen bonding in the adsorption mechanism. These findings highlight the potential of seaweed-derived biochar as an effective and eco-friendly solution for water purification.

Keywords: wastewater treatment; dye removal; biochar; seaweed biomass; carbonization

1. Introduction

Fresh water is a finite resource (3% of the Earth's water, of which only 0.5% is accessible) that is essential for life. In large-scale industrial applications, water pollutants must be removed before wastewater can be discharged into natural watercourses, as the legislation about the amount of pollutants is strict. Wastewater and water treatment is a market with considerable sales volume and great development potential in the next years (Figure 1) Wastewater treatment is seen as critical to environmental protection. There are several methods for removing pollutants from water. Table 1 summarizes the conventional, established, and emerging wastewater treatments, as well as their benefits and drawbacks [1]. Given the environmental importance of treating dye-contaminated wastewater, numerous technologies have been extensively studied in recent years. Bilal et al. [2] highlight various methods, including photocatalysis, ozonation, incineration, electrochemistry, ion exchange,

flocculation, electrocoagulation, micro-flocculation, electrocatalysis, catalytic photodegradation, advanced oxidation, membrane technologies, and biological processes. However, the authors emphasize that the key limitations of these emerging technologies—such as low removal efficiency, the generation of toxic byproducts, high energy demands, complex regeneration processes, and high costs—have led to a growing reliance on adsorption using biologically derived materials, such as biomass-based charcoal, for dye removal from wastewater.

Table 1. Existing and emerging processes to remove dyes from wastewater (adapted from [1]).

	Technology	Advantages	Disadvantages
Conventional	Coagulation Flocculation Biodegradation	Simple, economically feasible Economically attractive, publicly acceptable treatment	High sludge production, handling and disposal problems Slow process, necessary to create an optimal favorable environment, maintenance and nutrition requirements
	Adsorption on activated carbons	The most effective adsorbent, great, capacity, produces a high-quality treated effluent	Ineffective against disperse and vat dyes, the regeneration is expensive and results in loss of the adsorbent, non-destructive process
Established	Membrane separations	Removes all dye types, produces a high-quality treated effluent	High pressures, expensive, incapable of treating large volumes
	Ion-exchange	No loss of sorbent on regeneration, effective	Economic constraints, not effective for disperse dyes
	Oxidation	Rapid and efficient process	High energy cost, chemicals required
Emerging	Advanced oxidation process	No sludge production, little or no consumption of chemicals, efficiency for recalcitrant dyes	Economically unfeasible, formation of by-products, technical constraints
	Selective bio-adsorbents	Economically attractive, regeneration is not necessary, high selectivity	Requires chemical modification, non-destructive process
	Biomass	Low operating cost, good efficiency and selectivity, no toxic effect on microorganisms	Slow process, performance depends on some external factors (pH, salts)

The increasing use of dyes in the textile, cosmetics, leather, food, pharmaceutical, paint and varnish, and paper industries makes their removal in wastewater treatment processes crucial. Adsorption is the most frequently documented (Figure 2) of the several dye removal processes that have been investigated in the literature [3]. Sorbent materials' competitiveness in comparison to other pollution removal strategies is determined by the production and use costs. According to recently published data sorbent materials costs should be between 1 USD and 200 USD per mole of pollutant eliminated (cheap and expensive) [4].
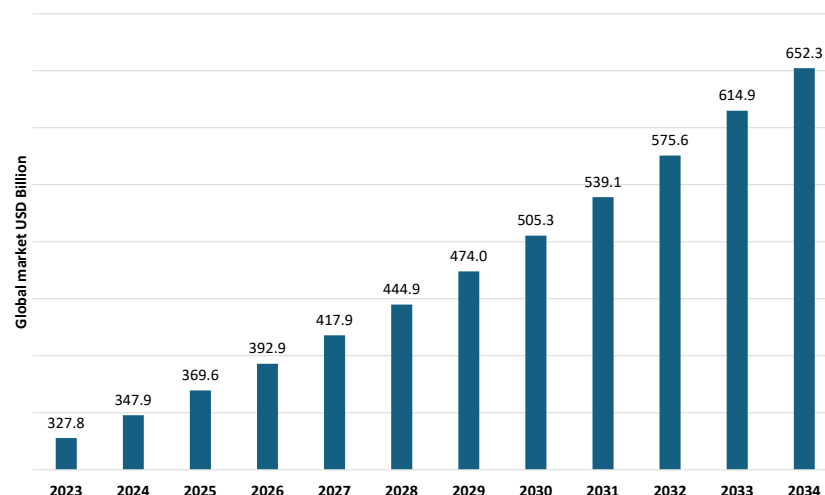
Figure 1. Global water and wastewater treatment market size 2023–2034 (data from [5]).

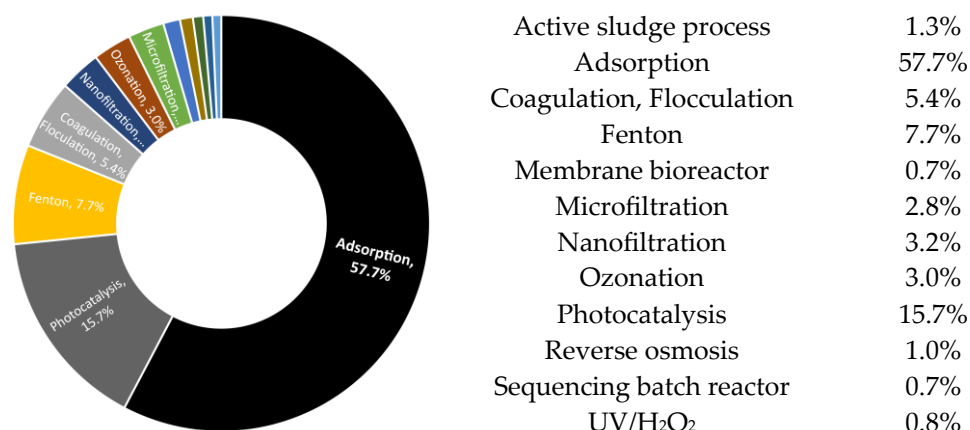|	
Active sludge process	1.3%
Adsorption	57.7%
Coagulation, Flocculation	5.4%
Fenton	7.7%
Membrane bioreactor	0.7%
Microfiltration	2.8%
Nanofiltration	3.2%
Ozonation	3.0%
Photocatalysis	15.7%
Reverse osmosis	1.0%
Sequencing batch reactor	0.7%
UV/H_2O_2	0.8%

Figure 2. Dyes removal from wastewater methods (adapted from [3]).

Sorbent materials' competitiveness in comparison to other pollution removal strategies is determined by the production and use costs. According to recently published data, the cost of sorbent materials should be between 1 USD and 200 USD per mole of pollutant eliminated (cheap and expensive) [4]. The sustainability of the water treatment process is closely tied to the sustainability of the sorbent materials used. Biosorbents, due to their renewable nature and potential for biodegradation, emerge as the preferred choice for this purpose. Sorbents derived from biomaterials can be prepared using a wide range of materials, including waste, following different preparation methodologies, and can be used to remove water pollutants including dyes, heavy metals, radionuclides, and pharmaceuticals, among others.

Methylene blue adsorption onto BC is a complex process embracing multiple mechanisms such as hydrogen bonding, electrostatic attraction, ion exchange, surface complexation, π interactions, and pore filling [6]. The morphology of biochar and the functional groups on its surface, with heteroatoms, play a crucial role in its ability to remove pollutants, as shown in Figure 3. The characteristics of biochar depend on the raw biomass, carbonization procedure, and post-production activation treatments [7]. The chemical properties of BC are determined by the C, H, N, S, and O content of the biomass that gives rise to it and factors in the production process, such as temperature. The most important physical property of BC is the porosity that is formed by the removal of volatile matter during carbonization [8]. Terrestrial and marine biomass have different compositions, giving rise to chars with different properties. Since oceans and seas envelop approximately 71% of the Earth's surface, marine macroalgae possess an abundant biomass. The utilization of

marine biomass like macroalgae, known as blue carbon, is pivotal in fostering sustainable development by enhancing the circular economy and thereby aiding in climate change mitigation [9]. Unlike terrestrial biomass, seaweed predominantly stores carbon in the form of sugars instead of lignocellulosic compounds. This unique attribute allows marine biomass to undergo carbonization under mild conditions compared to woody terrestrial biomass. Additionally, the substantial presence of inorganic salts in seaweed catalyzes gasification, accelerating its conversion into carbon-rich compounds. Seaweed-derived biochar has several functional groups that make it suitable for removing pollutants and soil amendments [10].

Figure 3. Methylene blue adsorption mechanisms in biochar (adapted from [10]).

Jiang et al. [11] studied MB removal using NaOH-activated seaweed-derived biochar. From DFT (Density-functional theory) computations, the authors attributed the high adsorption capacity to the high biochar porosity and synergy effect between the different adsorption mechanisms (p–p stacking, cation–p interaction, and electrostatic interaction). Other researchers also studied the performances of seaweed biochar in the MB removal from contaminated water. Data in Table 2 show that MB removal efficiency increases raising the temperature at which biochar is prepared and activation procedure also plays a chief role in the MB adsorption performances.

Despite extensive research on macroalgae biochar production, knowledge gaps remain. In a recent review, Wang et al. [12] emphasized the significant potential of seaweed biochar due to its readily available and cost-effective biomass source, underlining the need for additional investigation into the production and activation of these biochar's, given that reported materials exhibit notably low porosity. Additionally, they stated that seaweed biochar's sustainability hinges on the possibility of efficient adsorbent regeneration.

The following sections present results on the use of biochar for dye removal from wastewater. Biochar was produced by carbonization of seaweed biomass similar to *Sargassum*, harvested from the Portuguese coastline. The most efficient material achieved an adsorption capacity of 500 mg of dye per gram of solid—a significant value given the simplicity of the sorbent preparation, which required neither high-temperature thermal activation nor chemical treatment. This study aligns with the United Nations Sustainable Development Goals (SDGs) 6 (Clean Water and Sanitation) and 12 (Responsible Consumption and Production). It underscores the growing scarcity of potable water, exacerbated by consumer-driven industries such as clothing manufacturing, where resilient dyes contribute to industrial wastewater pollution.

Table 2. MB removal using seaweed-derived biochar from literature.

Biomass	Temperature (°C)	Activation	Washing	q_{max} (mg/g) *	Reference
Laminaria digitata	400	-	-	117	[13]
Laminaria digitata	250	-	-	175	[13]
Enteromorpha prolifera	500	NaOH, 800 °C	HCl, H_2O	244	[11]
Ulva lactuca	700	$ZnCl_2$	HCl, H_2O	345	[14]
Gelidiella acerosa	800	-	HCl, H_2O	513	[15]
Enteromorpha prolifera * Oily sludge	700	KOH	HCl, H_2O	910	[16]

Note(s): * maximum adsorption capacity by Langmuir adsorption isotherm.

2. Experimental

The char sorbents were prepared by slow carbonization of a brown seaweed mixture (Table 3), collected in the coastal areas of Portugal. Different species of marine algae were collected by hand from Praia de Alpertuche, Setúbal (38°28′4.93″ N, 8°59′22.27″ W) on three different dates: 28 May 2022, 4 July 2022, and 5 November 2022, to guarantee a more representative sample of the collected marine algae. The experimental procedure is summarized in Figure 4 as a block diagram. This figure also presents the hypothesis of utilizing the carbonization gas to supply the energy required for the process and recovering coal washing water for fertilizer or agricultural phytochemical production. The washing water, enriched with minerals like potassium (K) and soluble organic compounds from sugar carbonization, holds potential for agricultural applications. However, these two stages are not analyzed in the following sections, as they are still under development.

The collected biomass was washed thoroughly with tap water to remove contamination with sand and seawater and then dried naturally in contact with atmospheric air (2 days). A sufficient amount of water was used to thoroughly remove all the sand from the biomass. Lisbon's tap water meets the European Community's quality standards [17] for drinking water, with an average pH of approximately 8.0. The biomass was further dried overnight in an oven at 60 °C to ensure an easily grindable material.

After grinding in a blade mill, the biomass was sieved and the fractions above 750 mm were subjected to a new grinding process. Carbonization in a muffle was carried out by wrapping 10 g of biomass in an envelope (with four layers, around 3 g), of aluminum foil (Figure 5), leaving a small hole for the gases formed to escape, thus maintaining a non-oxidizing atmosphere during the process. The char samples were prepared at 300 °C and 400 °C. The carbonization temperature was chosen from the thermal degradation profile under nitrogen flow. The thermogram was acquired at 20 °C/min, under N_2 flow, using a Netzsch STA490 PC thermobalance. An alumina crucible with 60 mg of the powdered *sargaço* was used.

Table 3. Species and phylum/class percentages (wt. %, dried) of the prepared *sargaço* mixture.

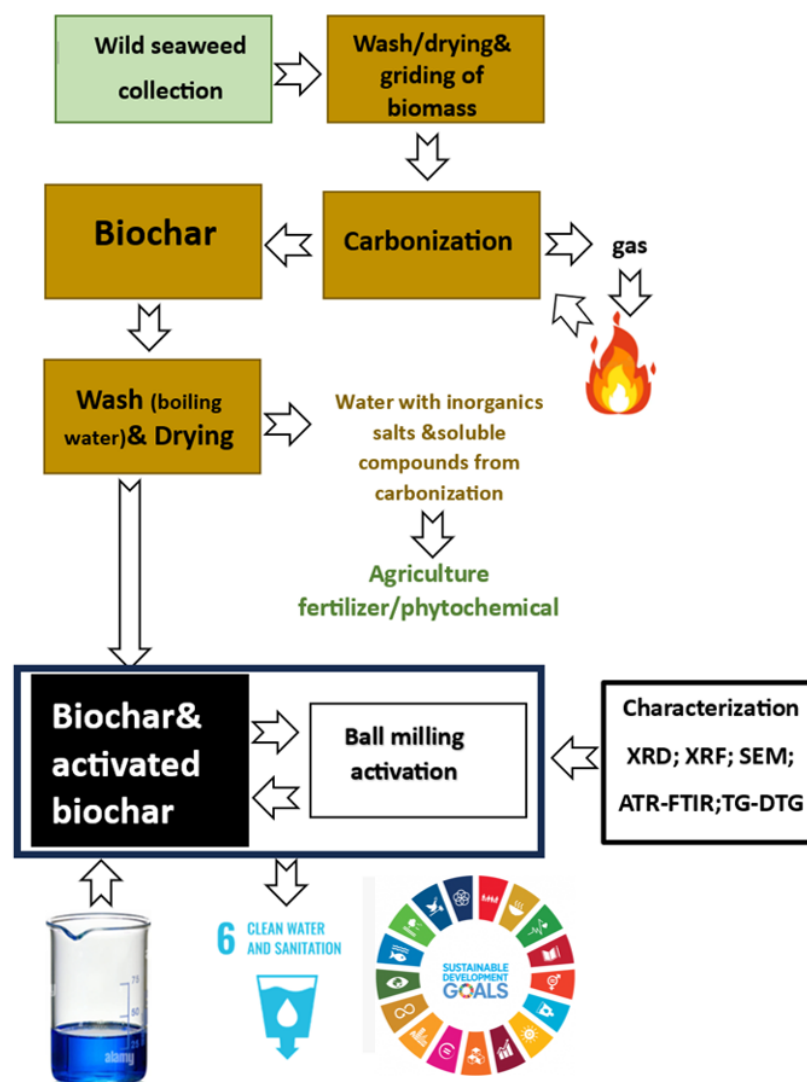| Phylum	Species	Species (wt. %; Dried)
Phaeophyceae	*Ascophyllum nodosum*	5.0
	Fucus vesiculosus	15.0
	Gongolaria baccata	10.1
	Saccorhiza polyschides	39.9
Chlorophyta	*Ulva lactuca*	7.5
	Ulva rigida	7.5
Rhodophyta	*Gelidium corneum*	7.0
	Gracilaria gracilis	4.0
	Plocamium cartilagineum	4.0

Figure 4. Schematic representation of the experimental procedure.

Figure 5. Aluminum foil envelope for biomass carbonization.

Previous research found that below 300 °C, the carbonized biomass contained a significant amount of water-soluble organic compounds, which is why this temperature was chosen as the lowest for the procedure. The consumption of energy is significantly over 400 °C, which is why this is the maximum temperature used. Heating during carbonization was carried out at a constant rate for a 2 h period and the sample remained at maximum temperature for 2 h. Cooling was performed slowly while keeping the sample inside the oven. After cooling, the chars were weighed and then washed with boiling distilled water

to remove water-soluble compounds formed during carbonization and inorganic salts. After filtration, the chars were dried overnight in an oven at 70 °C. The produced chars were labeled as S300 and S400, according to the carbonization temperatures, preceded by NW for unwashed and W for washed. The char prepared by carbonization at 400 °C was subjected to a physical activation treatment in a ball mill. The treatment was carried out for 1 h using Retsch S1 planetary ball mill equipment with the container and balls in agate (Retsch GmbH, Haan, Germany) using a ball/char mass ratio of around 10 and a rotational speed of 370 rpm. The ball/char volume ratio was 14/50 with balls of different diameters (six balls of 12 mm plus two balls of 20 mm). The pH of the prepared chars was determined in aqueous suspensions of the powdered materials following the methodology reported in the literature [18]. Briefly, a 1:20 (weight basis) suspension of solid in distilled water was prepared and kept under magnetic stirring (500 rpm) for 90 min. After the equilibration period, the pH was measured with a Consort C931 electrochemical analyzer (Consort, Turnhout, Belgium). The non-washed and washed chars were characterized by infrared spectroscopy to characterize the surface functional groups. The post-adsorption solids were also characterized to depict the interactions between the colorant molecules and the sorbent. The spectra were acquired by attenuated total reflectance mode using a PerkinElmer Spectrum Two IR spectrometer (PerkinElmer, Waltham, MA, USA) equipped with a Pike ATR accessory with a diamond crystal (PIKE Technologies, Madison, WI, USA).

Each spectrum was acquired in the 4000–600 cm^{-1} wavenumber range using four scans and a resolution of 4 cm^{-1}.

XRD was used to examine the inorganics in char materials as well as the chars themselves, both washed and unwashed. The diffractograms were plotted from 5 to 70° (step of 0.02° and 1 s by step) on a Bruker D8 Advance X-ray diffractometer (Bruker, Billerica, MA, USA) with Cu K_a radiation at 40 kV and 40 mA.

The morphology and near-surface chemical composition of the chars were assessed by SEM-EDS. Before analysis, the powdered sample was studded over a double-face carbon tape and covered by a thin film of Pd-Au. The micrographs were gathered using a Hitachi S-2400 Scanning Electron Microscope (Hitachi, Tokyo, Japan). The elemental analysis during image acquisition was performed using a Bruker light elements EDS detector at 20.0 kV.

The prepared chars were also characterized by Raman spectroscopy using a Horiba LabRam HR 800 Evolution confocal Raman micro spectrometer (Horiba Jobin Yvon, Kyoto, Japan) with a 532 nm laser focused with a $100\times$ objective with 10 mW power at the samples. The graphitization index (I_D/I_G) of the chars, was obtained by the curve fitting method applied to the spectral data in the 800–2000 cm^{-1} as reported before [19]. The I_D/I_G was obtained by the ratio of the areas under the Gaussian curves centered at 1367 cm^{-1} (D band) and 1587 cm^{-1} (G band). The G (graphitized material) band arises from the in-plane vibrations of SP_2 bonded carbon atoms while the D band is due to out-of-plane vibrations attributed to the presence of structural defects in disordered material [20].

The batch methylene blue adsorption tests were carried out in a thermostatic bath at temperatures in the 25 °C to 50 °C range. For each test, 50 mL of methylene blue solution (100 to 520.5 ppm) was previously thermostatic (15 min) in a stoppered flask with a magnetic stirrer. After the thermostabilization period, char (1 to 15 g/L) was added, and the adsorption test was conducted over a duration of 30 to 120 min. The reproducibility of the MB adsorption tests was tested using four replicates of a randomly chosen test. The associated error was computed using Student's distribution for a 95% confidence level. In the adsorption kinetics tests, samples were taken every 5 min during the first 30 min and every 15 min after that. After the adsorption tests, the char was removed by vacuum filtration, and the solid was dried in an oven (60 °C) overnight for subsequent characterization.

To optimize the sorbent dose used in adsorption experiments, various amounts of W-BM-S400 ranging from 0.05 to 0.75 g were added to 50 mL of solution at 40 °C. The impact of solution pH on MB adsorption was analyzed by adding HCl and/or NH$_4$OH until the desired pH (2–12) was achieved. The acid or base, in the form of concentrated solutions, was gradually added with continuous pH monitoring and vigorous stirring until the desired pH was achieved.

Adsorption experiments based on pH were conducted by adding 0.10 g of sorbent to 50 mL of MB solution at 40 °C. To investigate the influence of solution temperature on MB adsorption, 0.10 g of W-BM-S400 was added to 50 mL of MB solution at 25 °C, 30 °C or 40 °C. In all these experiments, the contact time was 30 min, the stirring speed was 900 rpm, and the MB solution concentration was 520.5 ppm.

The methylene blue in aqueous solutions was quantified using the UV-Vis spectroscopy. The calibration curve, absorbance versus MB concentration, was carried out for solutions with MB concentration in the 0–30 ppm range. As reported in the literature [21] the proportionality spectral feature/concentration was established for the absorbance at 664 nm. Figure 6 shows the UV-Vis spectra of standard solutions and the obtained calibration curve.
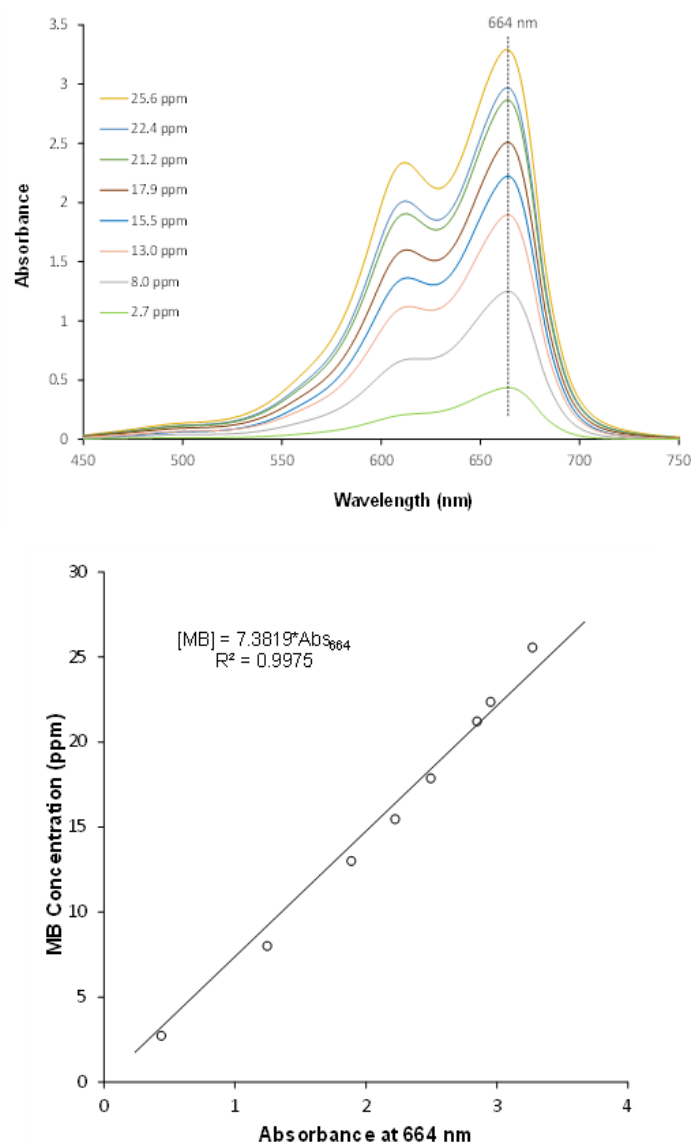

Figure 6. UV-Vis spectra and calibration curve for methylene blue quantification.

3. Results and Discussion

The *sargaço* biomass was characterized by thermogravimetry under N$_2$ flow to select the carbonization temperature. The thermal degradation profile in Figure 7 shows that at 400 °C the biomass has already suffered the greatest loss of mass, which occurs at a maximum rate of around 270 °C. Given the thermogravimetry data, 300 °C and 400 °C were chosen as the carbonization temperatures. The selected carbonization temperatures are in line with the data of Wang et al. [22], which show that the devolatilization stage of seaweed biomass occurs between 200 °C and 550 °C.
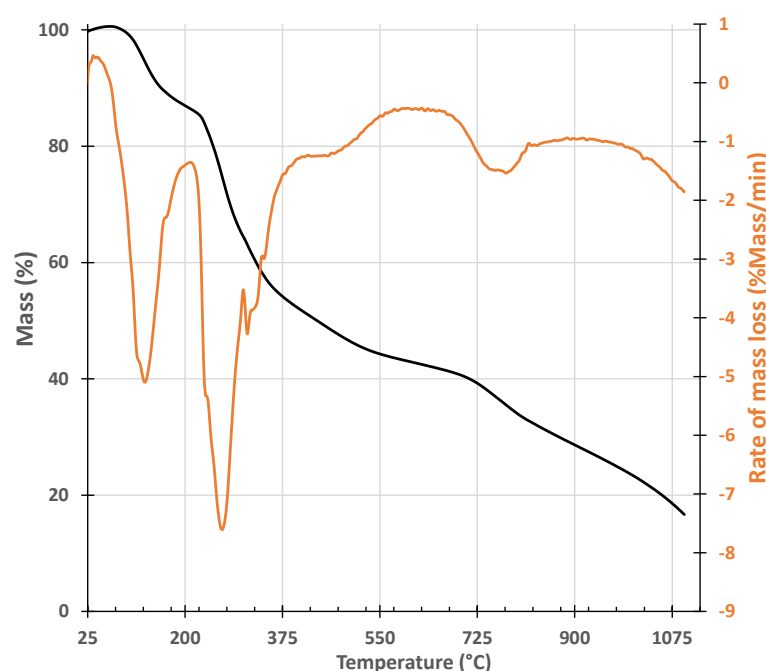

Figure 7. Thermogram of *sargaço* under N$_2$ flow with a heating rate of 20 °C/min.

After carbonization, the biomass was converted into a dark gray/black material with char yields and pH summarized in Table 4. The char yields agree with recently published data, which emphasizes that the yield depends on the carbonization temperature and the type of seaweed used [9]. The high content of alkali in seaweed biomass (Figure 8) can contribute to prompt gasification during carbonization thus decreasing the char yield [23]. All the prepared biochar presents an alkaline character due to inorganics, such as K, and the organic surface groups such as -COO- and -O- [24]. The biochar-washed samples present lower pH values due to the leaching of alkali salts.

Table 4. Yield (%) and pH of the produced char.

Biochar ID	Yield (%)	pH
NW-S300	57.4	8.5
W-S300	-	7.1
NW-S400	46.0	10.3
W-S400	-	9.3
NW-BM-S400	-	10
W-BM-S400	-	9.1

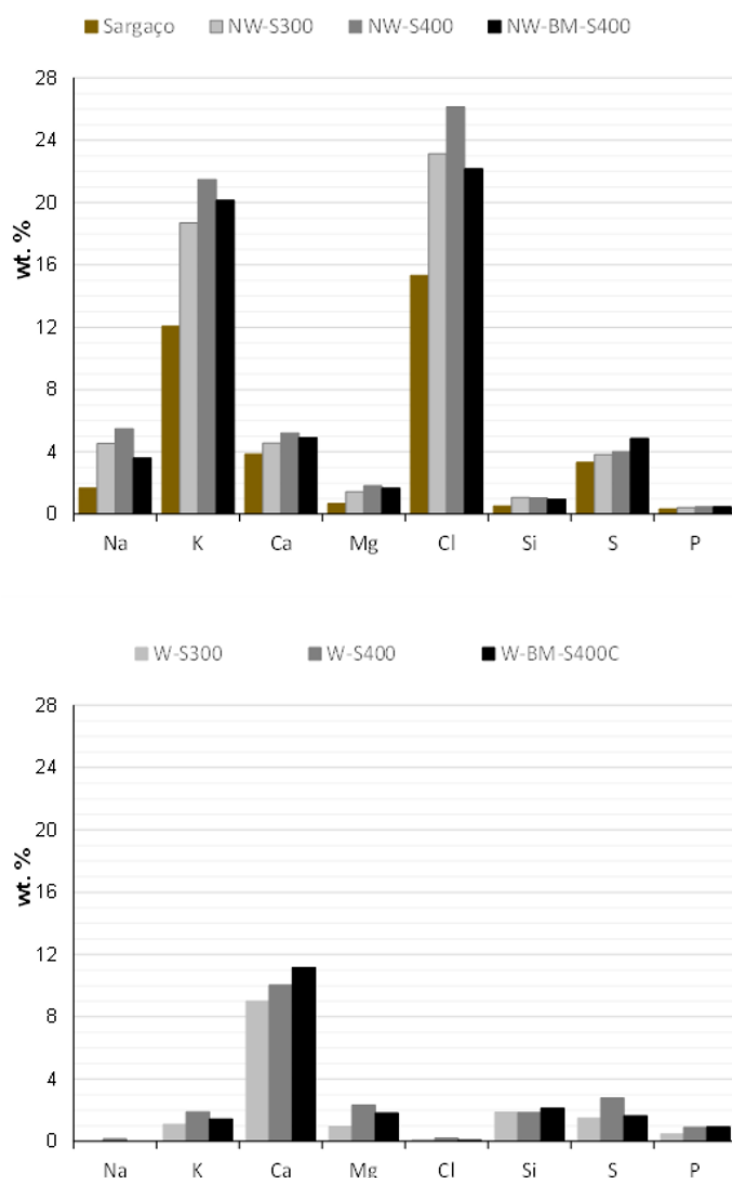Note(s): NW—non washed; W—washed; BM—ball milled; S—*sargaço*.

Figure 8. XRF elemental analysis of raw biomass and non-washed and washed char materials.

The high content of alkali elements of non-washed chars was confirmed by EDS during SEM micrographs acquisition (Figure 8). Both techniques, XRF and EDS, underline the fact that the washing procedure is crucial to leach inorganics salts of chars which would otherwise be solubilized in the wastewater to be treated. Results shown in Figures 8 and 9 indicate that Ca remains in the chars even after washing, which may contribute to better methylene blue adsorption. Wang et al. [25] reported that ion exchange and π–π stacking-π–π interactions in Figure 3-increased MB adsorption for Ca-modified rice husk chars. The ball-milled sample displays the highest Ca content.

The brownish-colored char washing water contained significant amounts of potassium and organic compounds resulting from the partial carbonization of algal sugars, making it a promising source of liquid fertilizer or foliar spray for agricultural and floricultural applications [26]. Inorganics in raw *sargaço* are well visible in SEM micrographs (Figure 10) as small agglomerates of light color studded over the bulk material. The leaching of alkali chlorides, and other water-soluble salts, during the washing procedure, was confirmed by X-ray diffraction (Figure 11). Non-washed samples show XRD patterns belonging to the inorganics crystalline phases whereas the char-washed sample's XRD lines of non-soluble-

inorganics such as quartz overlapped with the characteristic pattern of semi-graphitized char [27] with a broad feature centered at 23.5°.
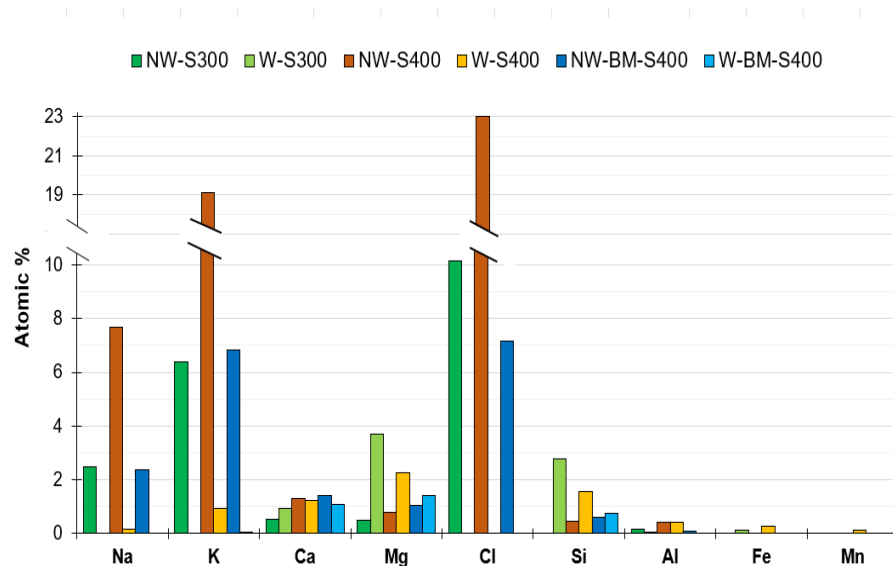

Figure 9. Inorganics in washed and non-washed biochar assessed by EDS.
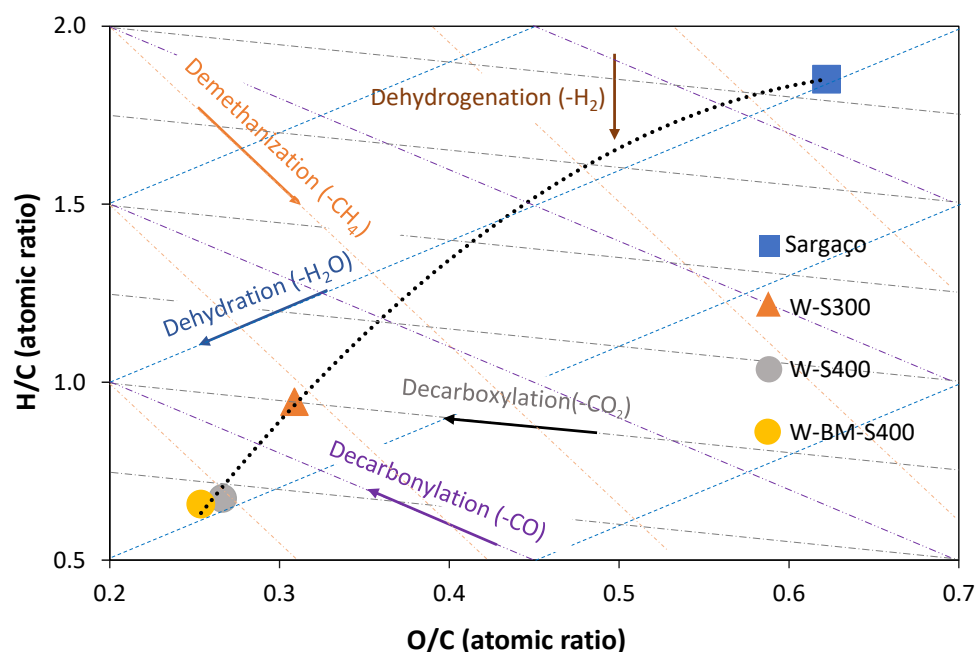

Figure 10. Van Krevelen diagram of raw biomass and prepared biochars.

The graphitization Index of the produced biochars was evaluated by Raman spectroscopy (Figure 12). Data from spectra deconvolution showed I_D/I_G values of 1.81, 1.70, and 1.67 for washed samples prepared at 300 °C, 400 °C, and ball mill, respectively. As expected, char graphitization increases raising the carbonization temperature [28] and ball milling also has a benefit on this char feature. In the spectral region between the D and G bands appears the D' band, around 1500 cm^{-1}, which results from defects induced by heteroatoms. This band results from the PAH (polycyclic aromatic hydrocarbons) moieties' combined vibration modes, mostly caused by N or O functional groups [29]. The ball-milled sample (W-BM-S400) exhibits a more intense D' band ($I_{D'}/I_D = 0.52$) compared to the other two samples (0.38 at 300 °C and 0.35 at 400 °C), indicating that the ball milling treatment promotes the formation of oxygen-containing functional groups. Moreover, such treatment

also increases the surface exposure of the preexistent functional groups [30]. The changes introduced by the ball milling occur through a radical mechanism [31] which allows rearrangements with the formation of aromatic groups with more units or termination with oxygenated groups.
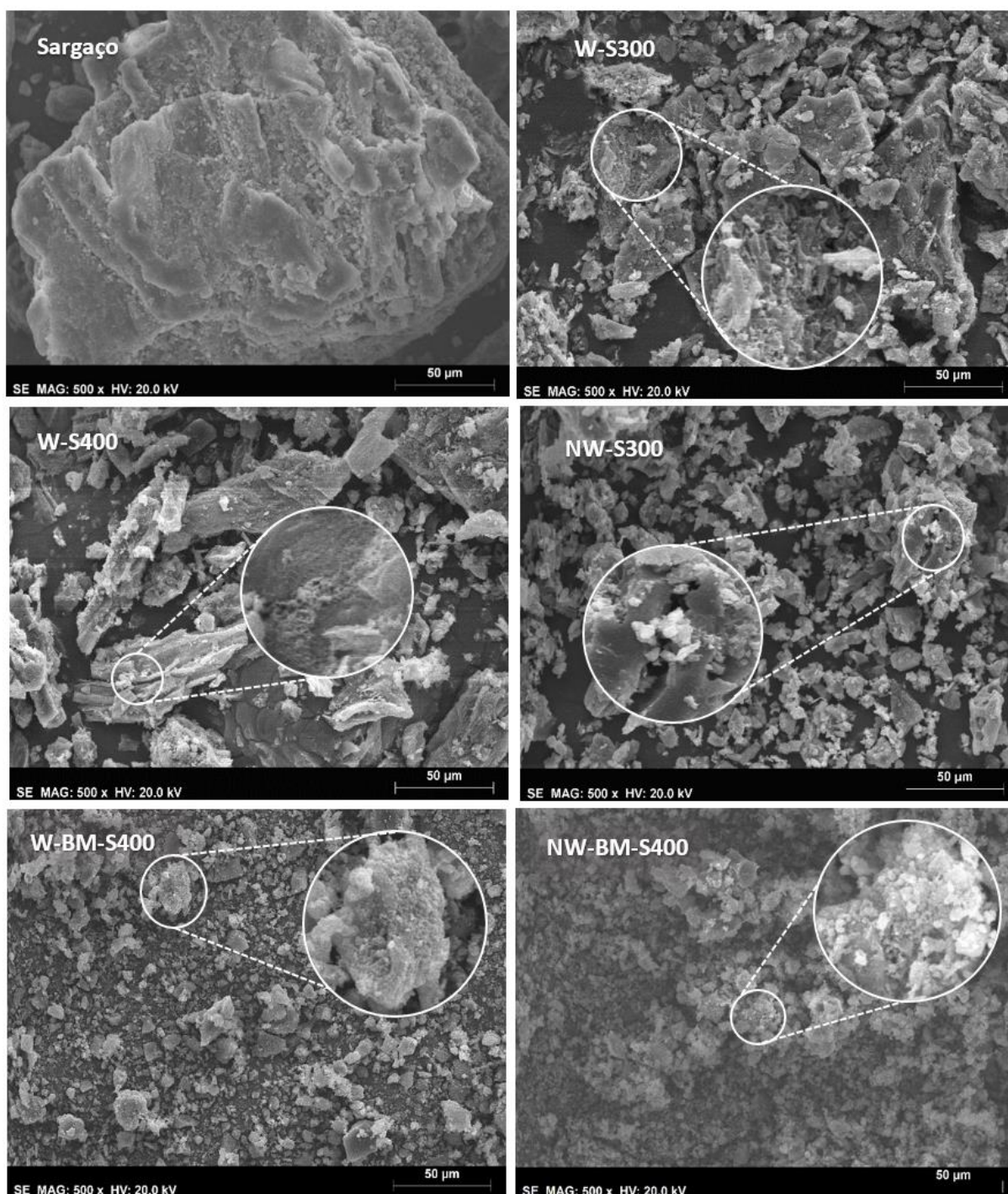

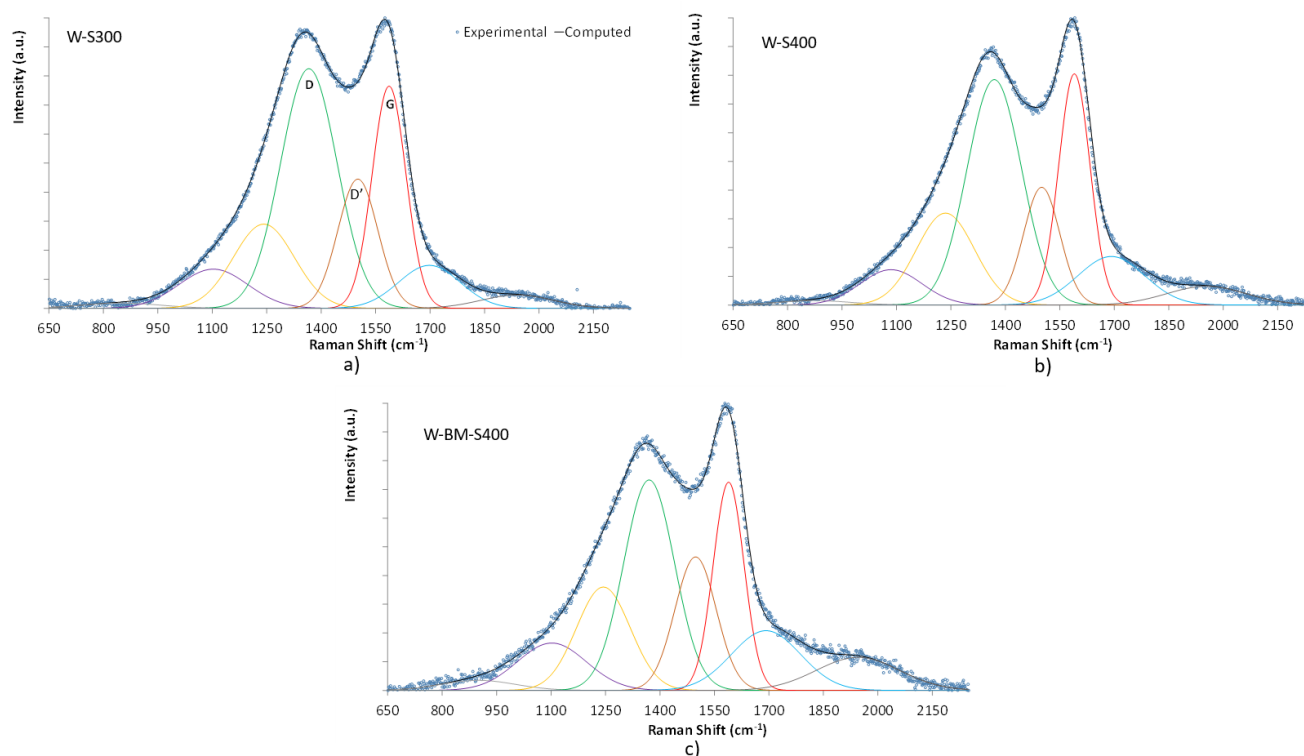**Figure 11.** SEM micrographs of *sargaço* and washed and non-washed chars.

Figure 12. Raman spectra of washed biochars (**a**–**c**). Experimental data were fitted using Gauss curves for bands D, D', G and other minor bands not discussed in this work.

The XRD data (Figure 13) also confirms the high inorganic content of biochar samples. The diffractograms show diffraction lines of alkali crystalline salts such as sylvite, halite, calcite, dolomite, and anhydrite overlapped with XRD lines belonging to quartz. The same XRD lines were observed for *sargaço* which is consistent with the high mineral content reported for the seaweed biomass [32]. Other researchers [33] reported a substantial inorganic content in seaweed-derived biochar, highlighting a key distinction from wood-derived biochar.

The O/C and H/C ratios, assessed by elemental analysis, of raw biomass and prepared biochars were used to draw the Van Krevelen diagram (Figure 10). This type of diagram facilitates the evaluation of the processes involved in biomass carbonization.

The predicted reaction path from raw biomass to chars, the dashed line, shows that the dehydration processes are dominant in the carbonization of *sargaço*, because the dehydration vector and the path are close. This observation is in line with what has been reported in the literature for the carbonization of sugars, which are the major components of seaweed [34]. As expected, higher carbonization temperature raises the loss of oxygen-containing species, decreasing the O/C ratio [35]. Ball milling for 1 h very slightly decreased O and H atomic percentages, and increased C atomic percentages, though it reduced H/C and O/C ratios (Figure 10). The same results were obtained by Timko et al. [31] studying glucose hydrothermal char.

Micrographs of non-washed char show inorganic materials agglomerates that are absent in washed chars. The morphology of char produced at 300 °C and 400 °C (Figure 11) by slow carbonization is less spongy than that reported in the literature for char produced by high-temperature pyrolysis (>600 °C), which implies a smaller surface area available for the adsorption of pollutants.
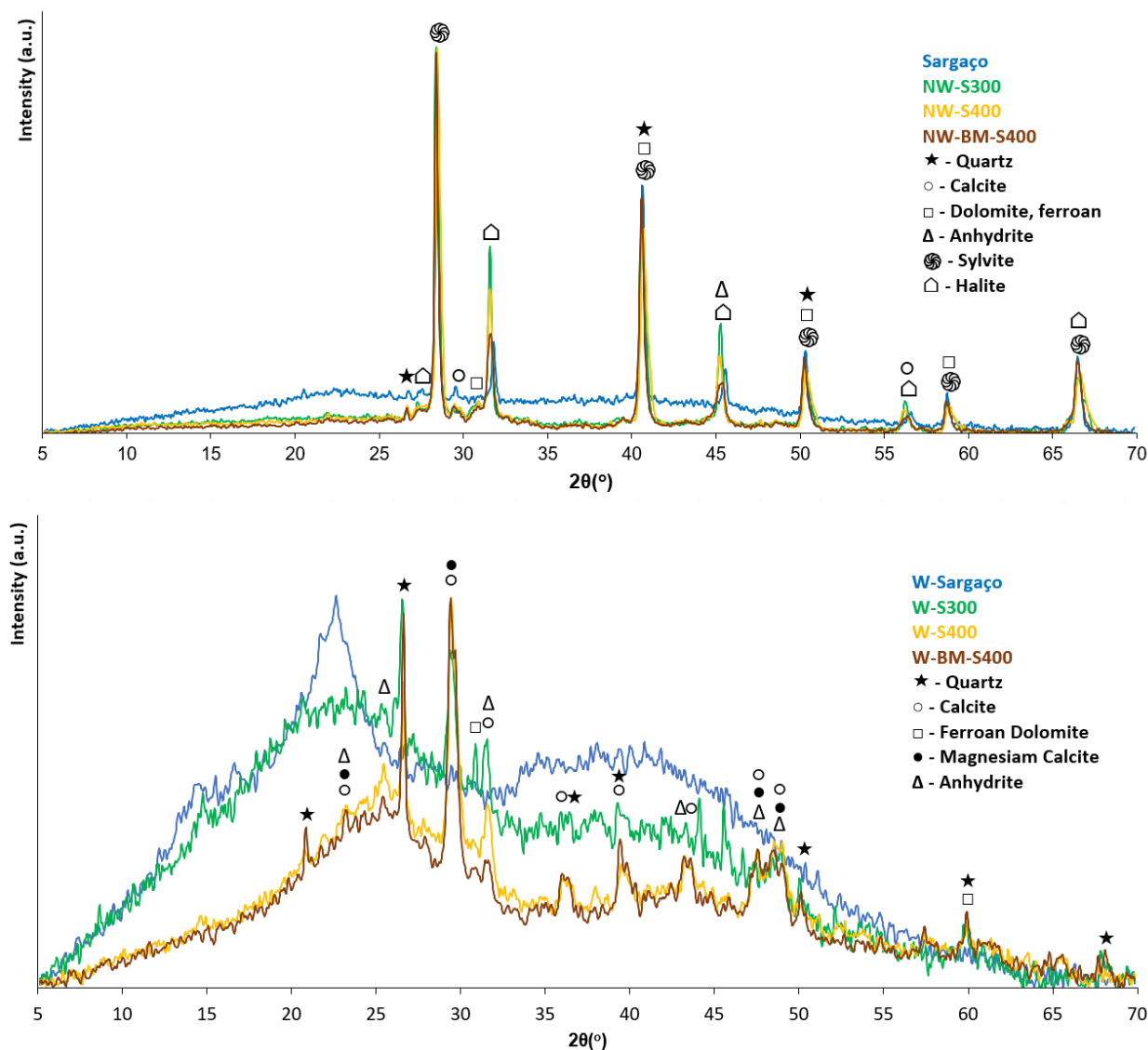
Figure 13. XRD patterns of washed and non-washed chars and raw biomass (*sargaço*).

The functional group on the char surface and the MB adsorbed species were evaluated by ATR-FTIR. Figure 14 presents the IR reflectance spectra of the biochars before MB adsorption, along with the raw biomass, with vibration mode assignments based on data from the literature.

The adsorption of MB onto the biochar was evaluated by comparing the shifts in the IR reflectance bands of pure MB with those observed in the biochar after adsorption (Table 5).

The data show that the band corresponding to the C-H vibration mode of the heterocycles is the one that undergoes the greatest shift, suggesting that the adsorption mechanism involves p–p interactions [36]. A kind of electrostatic interaction called the n–π interaction—in which the surface O and N contain functional groups whose atoms possess a lone pair of electrons, acting as electron donors and the aromatic rings in the biochar acting as electron acceptors [37,38]—could also have played a role in MB removal since the prepared chars contain considerable amounts of N and O.
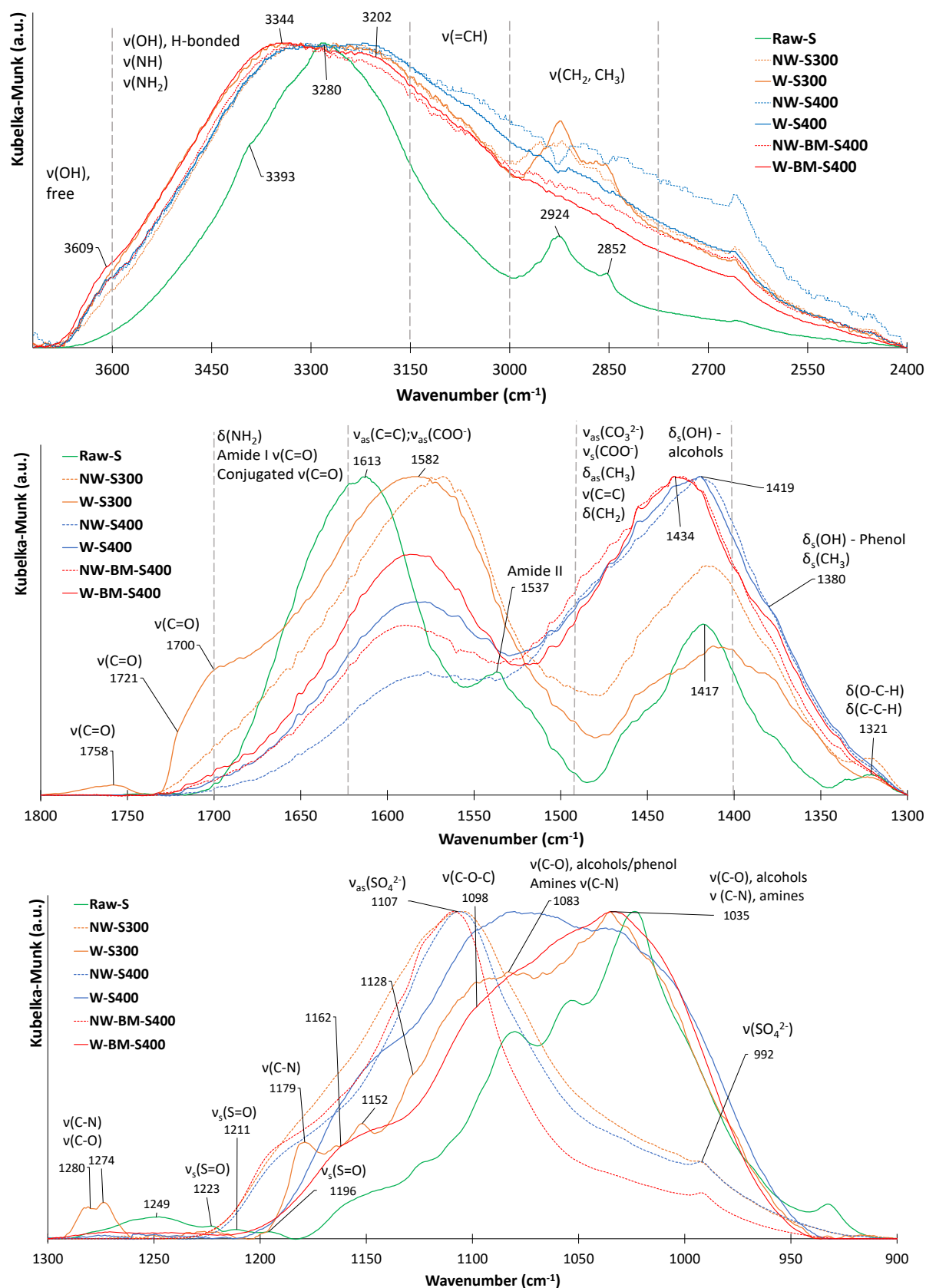
Figure 14. FTIR spectra of biochars before MB adsorption tests and raw biomass with vibration mode assignments based on data from the literature [36].

Table 5. FTIR bands of MB and MB adsorbed on chars and bands shift. Bands attribution according to Ovchinnikov et al. [36].

MB Solid (cm^{-1})	Char (cm^{-1})	Shift (cm^{-1})	Band Assignment in MB
3041	3058	+17	v_{het}(C-H)
2921	2921	0	ν_{as}(CH$_3$)
2850	2850	0	ν_s(CH$_3$)
1585	1596	+11	v_{het}(C=C), v_{het}(C=N)
1484	1489	+5	v_{het}(C=S$^+$)
1437	1437	0	δ_{as}(CH$_3$)
1382	1387	+4	δ(C-H), γ(C-H)
1349	1349	0	v(C=S$^+$)
1313	1327	+14	v(C-N), in N-CH$_3$
1244	1244	0	δ(C-H), γ(C-H)
1215	1223	+8	ν_{het}(C-C)
1162	1172	+10	δ_{het}(C-H)
1132	1134	+2	δ_{het}(C-N)
1036	1036	0	γ_{het}(C-H)
947	952	+5	N$_{het}\cdots$HO
876	884	+8	N$_{het}\cdots$HO
821	827	+6	δ_{het}(C-C)
666	668	+2	ν_s(C-S-C) in heterocycle

Note(s): v—stretching; δ—bending; s—symmetric vibration; as—asymmetric vibration; het—heterocycle.

For the MB adsorption tests, the char mass/solution volume ratio (dosage) was optimized using the sample produced at 400 °C and subjected to ball mill activation. For the 520.5 ppm MB solution (pH = 5.5) and 30 min adsorption period (Figure 15). In the tested conditions the MB removal efficiency increased raising the char mass due to the higher availability of adsorption sites. However, an increase in the adsorbent dose above 4 g/L, promoted a pronounced decrease in the MB adsorption capacity. A high dose of char could have blocked possible adsorption sites due to the superposition of the adsorbent layers. As a good practice, the char dose must be optimized to reach the highest MB removal efficiency while keeping the process cost-effective [3,39,40].
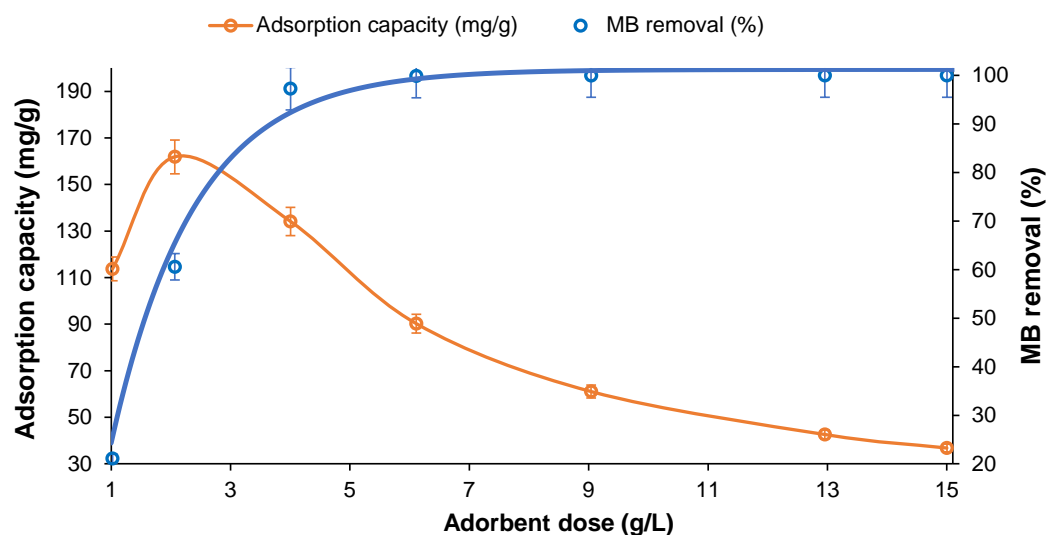
Figure 15. Effect of the adsorbent dosage on the adsorption capacity and MB removal (W-BM-400, 40 °C; [MB]$_o$ = 520.5 ppm).

The temperature effect was studied and the results in Figure 16 show that the char MB adsorption capacity increases with temperature, which is in line with thermodynamic

studies that indicate that the adsorption process is spontaneous and endothermic, i.e., favored by an increase in temperature [41].
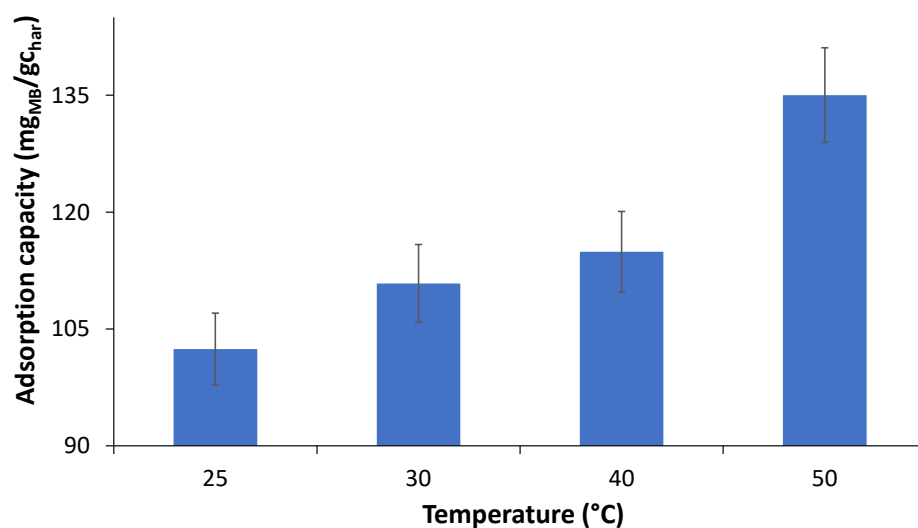

Figure 16. Temperature effect on the MB adsorption capacity (W-BM-400, dose = 2 g/L, [MB]$_o$ = 520.5 ppm).

The MB solution pH effect (Figure 17) on the char adsorption performances was studied using the char prepared at 400 °C with ball mill treatment which showed b FTIR few acidic O containing functional groups such as carboxylic acids. Thus, the pH-dependent electrostatic interaction between these functional groups conjugated bases negative charge and MB positive charge was not expected to play a huge role. The lower adsorption capacity at a pH of 2.2 was due to the increased competition between H$^+$ ions in solution and the cationic dye for adsorption sites on the char surface [25]. Moreover, the amine groups, detected by FTIR, can be protonated in acidic solutions, possessing a positive charge that repelled MB dye molecules. At pH in the 4.8–7.2 range, the adsorption capacity was almost the same, revealing that huge amounts of carbonate minerals of biochar have helped to remove H$^+$ from the solution [25,42]. Actually, after MB adsorption the initial pH of 4.8 changed to 7.4 [25]. The slightly higher adsorption capacity at a pH of 7.2 compared to a pH of 4.8 could have been due to some residual carboxylic acid groups which become deprotonated with a higher OH$^-$ presence in the solution, thus enhancing electrostatic interaction [13]. Despite the decrease in the electronegativity of char at lower pH and increased competition with H$^+$ for adsorption sites, the fairly good adsorption capacity obtained revealed that π–π interaction and hydrogen bonding must have been crucial for MB removal from solution [43]. As determined by the FTIR analysis strong shifts in the bands associated with MB interaction with biochar through H-bonding with N in methylamino groups and N in heterocycle were found. Moreover, the char had abundant aromatic structures on the surface, the π–π, interactions, n–π interactions, and Yoshida H-bonding have also been involved in MB adsorption.

At pH = 12.6, the methylene blue solution loses its distinctive blue hue and turns purple, indicating a structural shift in the molecule that appears to assist removal from the solution by adsorption onto the biochar. The literature claims that high pH aids in the removal of MB [44]. In any scenario, high pH values are prohibited from the standpoint of wastewater treatment process sustainability.
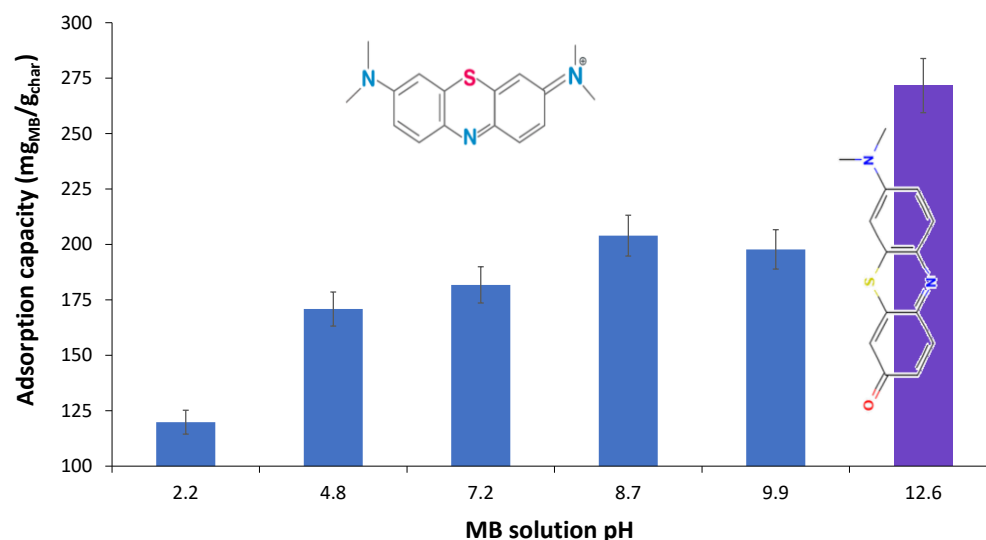
Figure 17. pH effect on the MB adsorption capacity (W-BM-S400, 2 g/L, 30 min; 40 °C and $[MB]_o = 520.5$ ppm).

Equilibrium data from the isothermal adsorption study at 40 °C were fitted using the Langmuir (Equation (1)) [45] and Freundlich (Equation (2)) isotherms (Figure 18).

$$q_e = \frac{q_{max}C_eK_L}{1 + C_eK_L} \tag{1}$$

$$q_e = K_F C_e^{\frac{1}{n_F}} \tag{2}$$

C_e—concentration of MB at equilibrium; q_e—the amount of adsorbate per mass unit of char at equilibrium; q_{max}—maximum monolayer adsorption capacity; K_L—Langmuir isotherm constant; K_F—Freundlich constant; and $\frac{1}{n_F}$—heterogeneity factor.
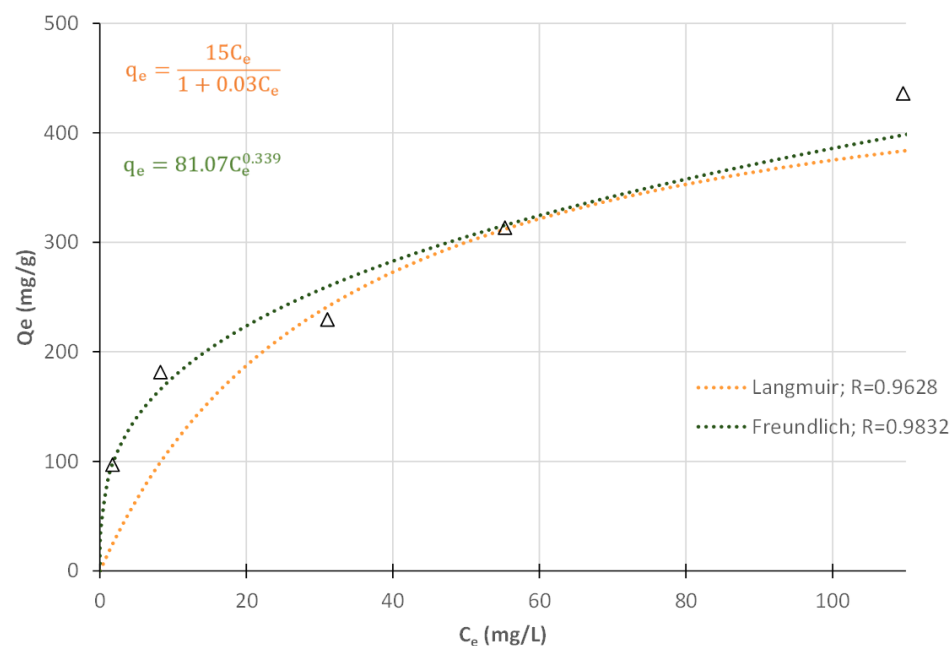

Figure 18. Langmuir and Freundlich adsorption isotherms, computed parameters, and correlation coefficients (R) for MB adsorption tests at 40 °C, and 2 $g_{biochar}$/L. (Δ—experimental data).

The Langmuir and Freundlich adsorption isotherms fitted to the MB adsorption data are shown in Figure 18. The same figure also presents the adjusted parameter values

for each isotherm, as well as the quality of the fit (R). The Freundlich model (R = 0.9832) provides a better fit than the Langmuir model (R = 0.9628). revealing that MB adsorption onto W-BM-S400 surface followed preferentially the Freundlich isotherm [14]. Thus, the surface of W-BM-S400 must be heterogeneous, in which MB dyes potentially auto associate to form multiple layers due to π–π stacking between dye monomers and H-bonds with solvent molecules (H_2O) [36].

Regarding the Langmuir isotherm, the obtained K_L value ranged between 0 and 1, confirming that the adsorption of MB dye onto W-BM-S400 was favorable [14,25]. Similarly, for the Freundlich isotherm, the heterogeneity factor ($1/n_F$) was lower than one, indicating that the adsorption process was favorable [36]. Additionally, the value of $1/n_F$ was less than 0.5, suggesting that MB was easily adsorbed [46]. From Langmuir model, the maximum computed adsorption capacity of the best prepared sorbent (400 °C, ball milled) was 500 mg_{MB}/g_{char}.

The maximum adsorption capacity of the prepared char is above the average values reported in the literature for char derived from terrestrial biomass, even when subjected to chemical/physical activation treatments (Figure 19).
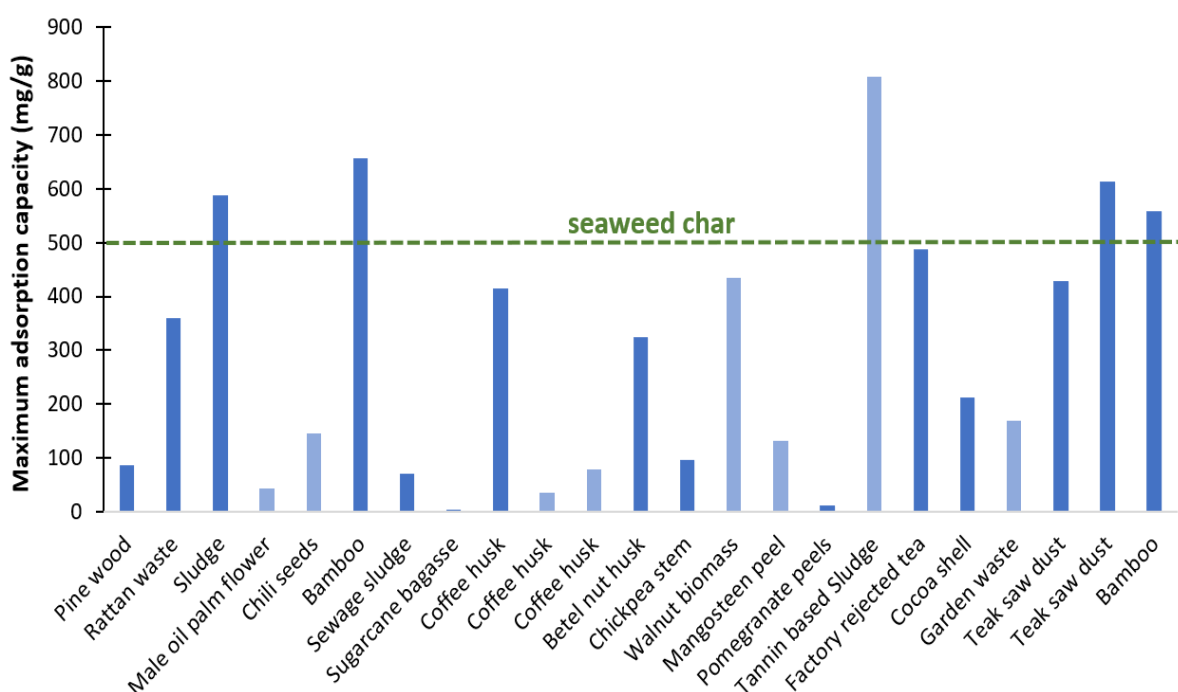

Figure 19. Maximum MB adsorption capacity of char compared with published data for land biomass-derived chars with (dark blue) and without activation treatment (light blue) (data source [47]). The green dotted line presents the maximum MB removal capacity for this work seaweed chars.

4. Conclusions

The invasive marine macroalgae that accumulate on beaches, causing environmental concerns, can be repurposed into carbonaceous materials such as biochar for wastewater treatment through adsorption. In this study, a mixture of seaweed, similar in composition to *sargaço* and harvested from the Portuguese coast, was carbonized at 300 °C and 400 °C to produce biochar for the removal of methylene blue (MB) from contaminated water. The resulting biochar, characterized by a low graphitization index and relatively compact morphology, underwent a washing process to remove alkali chlorides (K and Na), preventing solution contamination and ensuring that adsorption sites remained accessible. The remaining calcium salts in the biochar enhanced MB adsorption through an ion-exchange mechanism. The Freundlich isotherm parameters confirmed the heterogeneous nature

of the biochar surfaces and the favorability of MB adsorption ($\frac{1}{n_F} < 1$). Furthermore, the Langmuir isotherm adsorption kinetics revealed a maximum adsorption capacity of 500 mg MB/g char for the best-performing biochar. Notably, the adsorption capacity of these seaweed-derived biochar's exceeds the average reported for biochar's produced from woody biomass. Ball milling activation further enhanced adsorption performance. The promising results obtained in this study demonstrate that biochar's derived from seaweed, such as *Sargassum*, offer a sustainable and effective solution for removing dyes from wastewater, particularly from the fabric dyeing industry. This approach not only mitigates the environmental impact of algal overgrowth but also provides an eco-friendly alternative to conventional wastewater treatment methods. Future research should focus on biochar regeneration and reuse to evaluate its long-term feasibility for large-scale applications in industrial wastewater treatment.

Author Contributions: A.P.S.D.: conceptualization, resources, supervision, writing—original draft; F.A.S.: investigation, writing—original draft; B.R.: methodology, supervision, formal analysis, writing—review and editing; L.P.: resources, review and editing; D.C.S.: resources, review and editing; M.F.C.P.: resources, formal analysis, review and editing. All authors have read and agreed to the published version of the manuscript.

Abbreviations

BM	ball milled
C_e	concentration of MB at equilibrium;
K_F	Freundlich isotherm constant
K_L	Langmuir isotherm constant
MB	methylene blue dye
$\frac{1}{n_F}$	heterogeneity factor
NW	non washed char
q_e	amount of adsorbate per mass unit of char at equilibrium
Q^{max}	maximum monolayer adsorption capacity
S300	sargaço char produced at 300 °C
S400	sargaço char produced at 400 °C
Sargaço	Seaweeds harvested along the Portuguese coastline
W	washed char

References

1. Crini, G. Non-conventional low-cost adsorbents for dye removal: A review. *Bioresour. Technol.* **2006**, *97*, 1061–1085. [CrossRef] [PubMed]
2. Bilal, M.; Ihsanullah, I.; Hassan Shah, M.U.; Bhaskar Reddy, A.V.; Aminabhavi, T.M. Recent advances in the removal of dyes from wastewater using low-cost adsorbents. *J. Environ. Manag.* **2022**, *321*, 115981. [CrossRef] [PubMed]
3. Dutta, S.; Gupta, B.; Srivastava, S.K.; Gupta, A.K. Recent advances on the removal of dyes from wastewater using various adsorbents: A critical review. *Mater. Adv.* **2021**, *2*, 4497–4531. [CrossRef]
4. Ighalo, J.O.; Omoarukhe, F.O.; Ojukwu, V.E.; Iwuozor, K.O.; Igwegbe, C.A. Cost of adsorbent preparation and usage in wastewater treatment: A review. *Clean. Chem. Eng.* **2022**, *3*, 100042. [CrossRef]

5. Water and Wastewater Treatment Market Size to Hit USD 652.30 Billion by 2034. Available online: https://www.precedenceresearch.com/water-and-wastewater-treatment-market (accessed on 14 April 2025).

6. Singh, S.; Prajapati, A.K.; Chakraborty, J.P.; Mondal, M.K. Adsorption potential of biochar obtained from pyrolysis of raw and torrefied *Acacia nilotica* towards removal of methylene blue dye from synthetic wastewater. *Biomass Convers. Biorefinery* **2023**, *13*, 6083–6104. [CrossRef]

7. Yaashikaa, P.R.; Kumar, P.S.; Varjani, S.; Saravanan, A. A critical review on the biochar production techniques, characterization, stability and applications for circular bioeconomy. *Biotechnol. Rep.* **2020**, *28*, e00570. [CrossRef]

8. Jeyasubramanian, K.; Thangagiri, B.; Sakthivel, A.; Dhaveethu Raja, J.; Seenivasan, S.; Vallinayagam, P.; Madhavan, D.; Malathi Devi, S.; Rathika, B. A complete review on biochar: Production, property, multifaceted applications, interaction mechanism and computational approach. *Fuel* **2021**, *292*, 120243. [CrossRef]

9. Dang, B.T.; Ramaraj, R.; Huynh, K.P.H.; Le, M.V.; Tomoaki, I.; Pham, T.T.; Hoang Luan, V.; Thi Le Na, P.; Tran, D.P.H. Current application of seaweed waste for composting and biochar: A review. *Bioresour. Technol.* **2023**, *375*, 128830. [CrossRef]

10. Liu, S.; Shen, C.; Wang, Y.; Huang, Y.; Hu, X.; Li, B.; Karnowo; Zhou, J.; Zhang, S.; Zhang, H. Development of CO_2/H_2O activated biochar derived from pine pyrolysis: Application in methylene blue adsorption. *J. Chem. Technol. Biotechnol.* **2022**, *97*, 885–893. [CrossRef]

11. Jiang, D.; Li, H.; Cheng, X.; Ling, Q.; Chen, H.; Barati, B.; Yao, Q.; Abomohra, A.; Hu, X.; Bartocci, P.; et al. A mechanism study of methylene blue adsorption on seaweed biomass derived carbon: From macroscopic to microscopic scale. *Process Saf. Environ. Prot.* **2023**, *172*, 1132–1143. [CrossRef]

12. Wang, Y.; Ma, C.; Kong, D.; Lian, L.; Liu, Y. Review on application of algae-based biochars in environmental remediation: Progress, challenge and perspectives. *J. Environ. Chem. Eng.* **2023**, *11*, 111263. [CrossRef]

13. Güleç, F.; Williams, O.; Kostas, E.T.; Samson, A.; Stevens, L.A.; Lester, E. A comprehensive comparative study on methylene blue removal from aqueous solution using biochars produced from rapeseed, whitewood, and seeweed via different thermal conversion technologies. *Fuel* **2022**, *330*, 125428. [CrossRef]

14. El Nemr, A.; Shoaib, A.G.M.; El Sikaily, A.; Mohamed, A.E.D.A.; Hassan, A.F. Evaluation of Cationic Methylene Blue Dye Removal by High Surface Area Mesoporous Activated Carbon Derived from *Ulva lactuca*. *Environ. Process.* **2021**, *8*, 311–332. [CrossRef]

15. Ahmed, M.J.; Okoye, P.U.; Hummadi, E.H.; Hameed, B.H. High-performance porous biochar from the pyrolysis of natural and renewable seaweed (*Gelidiella acerosa*) and its application for the adsorption of methylene blue. *Bioresour. Technol.* **2019**, *278*, 159–164. [CrossRef] [PubMed]

16. Li, X.Y.; Han, D.; Xie, J.F.; Wang, Z.B.; Gong, Z.Q.; Li, B. Hierarchical porous activated biochar derived from marine macroalgae wastes (*Enteromorpha prolifera*): Facile synthesis and its application on Methylene Blue removal. *RSC Adv.* **2018**, *8*, 29237–29247. [CrossRef] [PubMed]

17. EUR-Lex-01998L0083-20151027-EN-EUR-Lex, (n.d.). Available online: https://eur-lex.europa.eu/legal-content/PT/TXT/?uri=CELEX:01998L0083-20151027 (accessed on 16 March 2025).

18. Singh, B.; Dolk, M.M.; Shen, Q.; Camps-Arbestain, M. Biochar pH, electrical conductivity and liming potential. In *Biochar: A Guide to Analytical Methods*; CSIRO Publishing: Clayton, Australia, 2017; pp. 23–38. Available online: https://ebooks.publish.csiro.au/content/ISBN/9781486305100 (accessed on 16 March 2025).

19. Rijo, B.; Dias, A.P.S.; Carvalho, J.P.S. Recovery of carbon fibers from aviation epoxy composites by acid solvolysis. *Sustain. Mater. Technol.* **2023**, *35*, 14–16. [CrossRef]

20. Brown, A.B.; McKeogh, B.J.; Tompsett, G.A.; Lewis, R.; Deskins, N.A.; Timko, M.T. Structural analysis of hydrothermal char and its models by density functional theory simulation of vibrational spectroscopy. *Carbon N. Y.* **2017**, *125*, 614–629. [CrossRef]

21. Fernandez-Perez, A.; Marban, G. Visible light spectroscopic analysis of methylene blue in water; what comes after dimer? *ACS Omega* **2020**, *5*, 29801–29815. [CrossRef]

22. Wang, S.; Zhao, S.; Uzoejinwa, B.B.; Zheng, A.; Wang, Q.; Huang, J.; Abomohra, A.E.F. A state-of-the-art review on dual purpose seaweeds utilization for wastewater treatment and crude bio-oil production. *Energy Convers. Manag.* **2020**, *222*, 113253. [CrossRef]

23. Soares Dias, A.P.; Rego, F.; Fonseca, F.; Casquilho, M.; Rosa, F.; Rodrigues, A. Catalyzed pyrolysis of SRC poplar biomass. Alkaline carbonates and zeolites catalysts. *Energy* **2019**, *183*, 1114–1122. [CrossRef]

24. Chung, B.Y.H.; Ang, J.C.; Tang, J.Y.; Chong, J.W.; Tan, R.R.; Aviso, K.B.; Chemmangattuvalappil, N.G.; Thangalazhy-Gopakumar, S. Rough set approach to predict biochar stability and pH from pyrolysis conditions and feedstock characteristics. *Chem. Eng. Res. Des.* **2023**, *198*, 221–233. [CrossRef]

25. Wang, K.; Peng, N.; Zhang, D.; Zhou, H.; Gu, J.; Huang, J.; Liu, C.; Chen, Y.; Liu, Y.; Sun, J. Efficient removal of methylene blue using $Ca(OH)_2$ modified biochar derived from rice straw. *Environ. Technol. Innov.* **2023**, *31*, 103145. [CrossRef]

26. Sangha, J.S.; Kelloway, S.; Critchley, A.T.; Prithiviraj, B. Seaweeds (Macroalgae) and Their Extracts as Contributors of Plant Productivity and Quality: The Current Status of Our Understanding. *Adv. Bot. Res.* **2014**, *71*, 189–219. [CrossRef]

27. Singh, M.; Vander Wal, R.L. Carbon Composites—Graphene-Oxide-Catalyzed Sugar Graphitization. *C* **2022**, *8*, 15. [CrossRef]

28. Yuan, R.; Dong, Y.; Hou, R.; Shang, L.; Zhang, J.; Zhang, S.; Chen, X.; Song, H. Structural transformation of porous and disordered carbon during ball-milling. *Chem. Eng. J.* **2023**, *454*, 140418. [CrossRef]

29. Ayiania, M.; Weiss-Hortala, E.; Smith, M.; McEwen, J.S.; Garcia-Perez, M. Microstructural analysis of nitrogen-doped char by Raman spectroscopy: Raman shift analysis from first principles. *Carbon N. Y.* **2020**, *167*, 559–574. [CrossRef]

30. Lopez-Tenllado, F.J.; Motta, I.L.; Hill, J.M. Modification of biochar with high-energy ball milling: Development of porosity and surface acid functional groups. *Bioresour. Technol. Rep.* **2021**, *15*, 100704. [CrossRef]

31. Timko, M.T.; Maag, A.R.; Venegas, J.M.; McKeogh, B.; Yang, Z.; Tompsett, G.A.; Escapa, S.; Toto, J.; Heckley, E.; Greenaway, F.T. Spectroscopic tracking of mechanochemical reactivity and modification of a hydrothermal char. *RSC Adv.* **2016**, *6*, 12021–12031. [CrossRef]

32. Soares Dias, A.P.; Rijo, B.; Santos, F.; Galhanos dos Santos, R.; Frade, T. Overview on biofuels production in a seaweed biorefinery. *Sci. Total Environ.* **2023**, *884*, 163714. [CrossRef]

33. Sun, J.; Norouzi, O.; Mašek, O. A state-of-the-art review on algae pyrolysis for bioenergy and biochar production. *Bioresour. Technol.* **2022**, *346*, 126258. [CrossRef]

34. Zhang, C.; Zhang, L.; Gao, J.; Zhang, S.; Liu, Q.; Duan, P.; Hu, X. Evolution of the functional groups/structures of biochar and heteroatoms during the pyrolysis of seaweed. *Algal Res.* **2020**, *48*, 101900. [CrossRef]

35. Bakshi, S.; Banik, C.; Laird, D.A. Estimating the organic oxygen content of biochar. *Sci. Rep.* **2020**, *10*, 13082. [CrossRef] [PubMed]

36. Ovchinnikov, O.V.; Evtukhova, A.V.; Kondratenko, T.S.; Smirnov, M.S.; Khokhlov, V.Y.; Erina, O.V. Manifestation of intermolecular interactions in FTIR spectra of methylene blue molecules. *Vib. Spectrosc.* **2016**, *86*, 181–189. [CrossRef]

37. Zhang, X.; Wang, Y.; Cai, J.; Wilson, K.; Lee, A.F. Bio/hydrochar Sorbents for Environmental Remediation. *Energy Environ. Mater.* **2020**, *3*, 453–468. [CrossRef]

38. Gayathri, K.; Palanisamy, N. Methylene blue adsorption onto an eco-friendly modified polyacrylamide/graphite composites: Investigation of kinetics, equilibrium, and thermodynamic studies. *Sep. Sci. Technol.* **2020**, *55*, 266–277. [CrossRef]

39. Enaime, G.; Baçaoui, A.; Yaacoubi, A.; Lübken, M. Biochar for Wastewater Treatment—Conversion Technologies and Applications. *Appl. Sci.* **2020**, *10*, 3492. [CrossRef]

40. Barquilha, C.E.R.; Braga, M.C.B. Adsorption of organic and inorganic pollutants onto biochars: Challenges, operating conditions, and mechanisms. *Bioresour. Technol. Rep.* **2021**, *15*, 100728. [CrossRef]

41. Li, H.; Kong, J.; Zhang, H.; Gao, J.; Fang, Y.; Shi, J.; Ge, T.; Fang, T.; Shi, Y.; Zhang, R.; et al. Mechanisms and adsorption capacities of ball milled biomass fly ash/biochar composites for the adsorption of methylene blue dye from aqueous solution. *J. Water Process Eng.* **2023**, *53*, 103713. [CrossRef]

42. Yang, C.; Miao, S.; Li, T. Influence of water washing treatment on *Ulva prolifera*-derived biochar properties and sorption characteristics of ofloxacin. *Sci. Rep.* **2021**, *11*, 1797. [CrossRef]

43. Lyu, H.; Gao, B.; He, F.; Zimmerman, A.R.; Ding, C.; Tang, J.; Crittenden, J.C. Experimental and modeling investigations of ball-milled biochar for the removal of aqueous methylene blue. *Chem. Eng. J.* **2018**, *335*, 110–119. [CrossRef]

44. Zhu, Y.; Yi, B.; Yuan, Q.; Wu, Y.; Wang, M.; Yan, S. Removal of methylene blue from aqueous solution by cattle manure-derived low temperature biochar. *RSC Adv.* **2018**, *8*, 19917–19929. [CrossRef] [PubMed]

45. Mani, D.; Elango, D.; Priyadharsan, A.; Al-Humaid, L.A.; Al-Dahmash, N.D.; Ragupathy, S.; Jayanthi, P.; Ahn, Y.H. Groundnut shell chemically treated with KOH to prepare inexpensive activated carbon: Methylene blue adsorption and equilibrium isotherm studies. *Environ. Res.* **2023**, *231*, 116026. [CrossRef]

46. Liu, L.; Li, Y.; Fan, S. Preparation of KOH and H_3PO_4 Modified Biochar and Its Application in Methylene Blue Removal from Aqueous Solution. *Processes* **2019**, *7*, 891. [CrossRef]

47. Sivaranjanee, R.; Kumar, P.S.; Rangasamy, G. A critical review on biochar for environmental applications. *Carbon Lett.* **2023**, *33*, 1407–1432. [CrossRef]